International Journal of Heat and Fluid Flow 120 (2026) 110307

Contents lists available at ScienceDirect

International Journal of Heat and Fluid Flow

journal homepage: www.elsevier.com/locate/ijhff

Modified scaling for turbulent heat transfer on rough surfaces

R. Gaudioso [a,b,*], D. Sotomayor-Zakharov [a], M. Gallia [a]

[a] Institute of Fluid Mechanics, TU Braunschweig, Hermann-Blenk Str. 37, Braunschweig, 38118, Lower Saxony, Germany
[b] Department of Aerospace Science and Technology, Politecnico di Milano, Via La Masa 34, Milan, 20156, Italy

ARTICLE INFO

Keywords:
Icing
Roughness
Convective heat transfer
Turbulent boundary layer
Reynolds analogy
LES
DNS

ABSTRACT

This study proposes a modified scaling for turbulent heat transfer on rough walls. The formulation introduces modified friction quantities u_τ^* and T_τ^*, exploiting a non-dimensional parameter G. Directly computed from simulations, G enters the Reynolds analogy and reflects the absence of a heat-transfer counterpart to local pressure gradients. Two numerical databases at comparable $Pr \sim 0.7$ are examined: a periodic channel DNS over sinusoidal roughness, and a turbulent thermal boundary layer LES over irregular ice roughness. Despite their differing topologies, both reveal a proportionality between G and the roughness Stanton number St_k^{-1}. A relation was fitted that provides accurate St estimates and supports the interpretation of G as a measure of thermal resistance relative to momentum transfer, similarly to St_k^{-1}. Furthermore, a correction to the classical $\Delta\Theta^+(k_s^+)$ scaling, based on G, yields improved collapse of temperature and velocity log-layer shifts. The results indicate that G could be potentially used to extend Reynolds analogy models based on the proposed scaling. While being limited to specific roughness datasets and flow conditions, this framework offers a first step towards an alternative numerical modeling of heat transfer in rough-wall turbulence.

1. Introduction

Heat transfer in turbulent flows over rough surfaces plays a central role in both natural and industrial contexts. Compared to momentum transport and skin friction, however, the effects of roughness on turbulent heat transfer have received much less attention (Kadivar and Garg, 2025). Current understanding is still largely based on statistical and phenomenological theories (Zhong et al., 2023), supported by experimental measurements and high-fidelity simulations such as Direct Numerical Simulation (DNS) and Large-Eddy Simulation (LES).

DNS of smooth-wall flows (Kasagi et al., 1992; Pirozzoli et al., 2016) show strong correlations between wall heat flux and temperature fluctuations, and between wall shear stress and velocity fluctuations. For $Pr \sim 1$ at sufficiently high Reynolds numbers, once the viscous sublayer is negligible compared to the log-layer, Kadivar and Garg (2025) observe that the ratio of turbulent timescales of velocity and temperature fluctuations remains nearly constant, despite differences in large-scale structures. This motivates the Reynolds analogy, which assumes that heat and momentum transfer are governed by the same turbulent eddies in the log-layer, yielding

$$RA = \frac{2St}{c_f} = Pr^{-2/3}, \tag{1}$$

also known as the Chilton–Colburn analogy, with $RA = 1$ for $Pr = 1$. The analogy assumes a turbulent Prandtl number $Pr_t = 1$. While this is approximately valid in the logarithmic layer of smooth walls, where $Pr_t \approx 0.85$–0.9 (Pirozzoli et al., 2016), the value can change abruptly near the wall and in presence of roughness (Hantsis and Piomelli, 2022; MacDonald et al., 2019). Nevertheless, following Townsend's outer-layer similarity hypothesis (Townsend, 1976), smooth and rough-wall Pr_t profiles are expected to collapse in the log-layer. At small scales, heat transfer is dominated by molecular conduction, whereas momentum transfer remains turbulence-driven, limiting the analogy (Kays and Crawford, 1993; Dipprey and Sabersky, 1963). Consequently, the Chilton–Colburn analogy is most accurate for smooth-wall flows with $0.6 < Pr < 60$ and deteriorates in the presence of strong pressure gradients.

This limitation becomes even more pronounced for rough surfaces, where protrusions generate wakes and localized pressure gradients. Unlike momentum transfer, where drag can be decomposed into viscous and pressure contributions, there is no analogous partition for convective heat transfer (Kadivar and Garg, 2025; Zhong et al., 2023; Bons, 2005). As a result, the applicability of the Reynolds analogy to rough walls is inherently restricted. To overcome this, various rough-wall heat-transfer models have been developed. An updated and detailed review of various applications can be found in Kadivar and Garg (2025), which distinguish two main modeling approaches. The first is based on the Cavity-Vortex (CV) hypothesis elaborated

* Corresponding author at: Institute of Fluid Mechanics, TU Braunschweig, Hermann-Blenk Str. 37, Braunschweig, 38118, Lower Saxony, Germany.
E-mail address: riccardo.gaudioso@tu-braunschweig.de (R. Gaudioso).

https://doi.org/10.1016/j.ijheatfluidflow.2026.110307
Received 7 November 2025; Received in revised form 3 February 2026; Accepted 7 February 2026
Available online 15 February 2026

Nomenclature

English symbols

B	Fully-rough regime constant
C, C_θ	Law of the wall constants
c_f	Skin friction coefficient
c_P	Specific heat at constant pressure [J/(kg K)]
d	Virtual rough wall origin [m]
e_r, e_τ	Relative % errors
G	Ratio of friction velocities
g_k	Roughness similarity function
h	Half turbulent channel height [m]
k	Roughness local height [m]
k_a	Roughness amplitude (sinusoidal surface) [m]
k_m	Roughness mean height [m]
k_s	Equivalent sand grain roughness [m]
k_z	Roughness peak-to-valley height [m]
L	Reference length [m]
m, c	Cavity Vortex model exponents
p	Static pressure [Pa]
Pr, Pr_t	Molecular and turbulent Prandtl number
q_w	Convective heat flux at wall [W/m^2]
R_q	Roughness root-mean-square height [m]
RA	Reynolds Analogy factor
Re, Re_τ	Reynolds number and friction Reynolds number
S	Surface area [m^2]
Sk	Roughness skewness
St, St_k	Stanton number and roughness Stanton number
T	Temperature [K]
T_τ, T_τ^*	Classic and viscous-based friction temperature [K]
U_∞	Reference inflow velocity [m s$^-$1]
u_τ, u_τ^*	Classic and viscous-based friction velocity [m s^{-1}]
y_c	Wall distance for evaluation of roughness shifts [m]
ES	Surface effective slope
$\boldsymbol{u} = (u, v, w)$	Velocity vector and its Cartesian components [m s^{-1}]
$\boldsymbol{x} = (x, y, z)$	Position vector and its Cartesian components [m]

Greek symbols

α_k, α_c	Cavity Vortex model constant
$\boldsymbol{\eta}$	Rough surface outward normal vector
$\Delta\Theta^+$	Roughness temperature log-layer shift in wall-units
ΔU^+	Roughness velocity log-layer shift in wall-units
κ	von Kármán constant
Λ	Rough surface wavelength [m]
λ	Air thermal conductivity [W/(m K)]
μ	Dynamic viscosity [Pa s]
ν	Kinematic viscosity [m^2/s]
ρ	Density [kg m^{-3}]
τ	Viscous shear stress component [Pa]
τ_v	Viscous shear stress magnitude [Pa]
τ_w	Total wall shear stress [Pa]
θ	Passive scalar, relative wall-temperature [K]

Abbreviations

CV	Cavity-Vortex model
DNS	Direct Numerical Simulation
LES	Large-Eddy Simulation
RANS	Reynolds-Averaged Navier–Stokes

Subscripts/Superscripts/Operators

$(\cdot)^+$, $(\cdot)^*$	Classic and modified wall-units scaling
$(\cdot)_n$	Local surface element quantity
$(\cdot)_w$	Wall-related quantity
$(\cdot)_{b/f}$	Bulk and/or full-channel quantity
$(\cdot)_{x,y,z}$	Spatial components
$\langle(\cdot)\rangle$	Double-average
$\overline{(\cdot)}$	Time-average

by Dipprey and Sabersky (1963) and Owen and Thomson (1963), while a second approach follows the so-called surface renewal (Kolmogorov–Brutsaert) theory, initially proposed by Brutsaert (1975) using the Kolmogorov's energy-cascading concept of turbulent eddies to describe local heat transfer in turbulent boundary layers.

For turbulence modeling applications, the geometrical effect of roughness is introduced in RANS solvers via the equivalent sand-grain height k_s, which incorporates the impact of surface protrusions through log-law modifications of velocity and temperature (or transported scalar) profiles (Kadivar et al., 2021). These modifications are typically expressed as log-layer shifts ΔU^+ and $\Delta\Theta^+$:

$$u^+ = \frac{1}{\kappa}\log y^+ + C - \Delta U^+, \tag{2}$$

$$\theta^+ = \frac{Pr_t}{\kappa}\log y^+ + C_\theta - \Delta\Theta^+, \tag{3}$$

with $\kappa \simeq 0.4$ the von Kármán constant, $C = 5$, and $C_\theta = 13.2Pr - 5.34$. In this context, the "+" superscript indicates wall-units scaling using the classic definitions of friction velocity $u_\tau = \sqrt{\tau_w/\rho}$ and friction temperature $T_\tau = q_w/(\rho c_P u_\tau)$, being τ_w the total shear stress at the wall (including pressure shear), q_w the total heat flux at the wall, ρ the fluid density, and c_P its specific heat at constant pressure. Wall-distance is scaled as $y^+ = (y-d)u_\tau/\nu$, where ν is the fluid kinematic viscosity and d is the wall-virtual origin, which is shifted in presence of roughness. Several definitions of d exist in literature, implying different law-of-the-wall profile distributions (Kadivar and Garg, 2025). The roughness shifts provide a modeling framework to quantify the impact of roughness on mean turbulent properties. While ΔU^+ displays a clear dependence on k_s^+, especially in the fully rough regime across different roughness types (Flack and Schultz, 2010; Forooghi et al., 2017), the behavior of $\Delta\Theta^+$ is far less understood. Several studies (Zhong et al., 2023; MacDonald et al., 2019; Peeters and Sandham, 2019) have reported a halted growth of $\Delta\Theta^+$ at large k_s^+ in contrast to the continued increase of ΔU^+, suggesting a lag in heat-transfer enhancement relative to friction increase, driven by the disproportionate influence of pressure drag.

To address these challenges, recent numerical studies have employed LES and DNS of rough surfaces in canonical flow configurations.

DNS has been widely applied to periodic turbulent channel flows featuring irregular roughness (Thakkar et al., 2017; Forooghi et al., 2017; Yang et al., 2022, 2023). While extensive efforts have been dedicated to friction, fewer studies include scalar transport for thermal analysis. For example, Peeters and Sandham (2019) studied irregular random roughness effects on turbulent convection, demonstrating that increasing roughness protrusions lead to differences in temperature fluctuations with respect to velocity, and stating the breakdown of the Reynolds analogy on the analyzed surfaces. MacDonald et al. (2019) performed a similar analysis on sinusoidal roughness, by employing a minimal channel set-up, and noticing an improved analogy between the viscous part of the shear stress and heat flux at the wall. This was later confirmed in additional studies from Zhong et al. (2023) and Rowin et al. (2024), where the sensitivity of thermal effects to additional parameters such as Pr number and roughness solidity was investigated. Forooghi et al. (2018a,b) characterized heat transfer properties on a series of artificial and realistic roughness topologies, also proposing a modified RA model based on k_s^+. A series of LES investigations including heat transfer effects have been conducted on Additive-Manufactured (AM) rough surfaces in a pipe-flow configuration (Garg et al., 2024b,a). The findings evidenced a Reynolds analogy breakdown aligned with literature observations, as well as the deviating behavior of the thermal roughness function ($\Delta\Theta^+$) with respect to the momentum one (ΔU^+). However, a potential non-classical behavior in the fully rough regime for the heat transfer similarity function was found, demanding specific attention for such AM applications. Moreover, skewness effects were considered to have an impact on the surface heat transfer response, which has increased performance for peak-dominant surfaces. Turbulent friction and thermal effects on anisotropic, irregular roughness have been investigated by Yang et al. (2025) in the transitionally rough regime at $Re_\tau \sim 500$ and $Pr \sim 0.71$. The authors proposed a combined parameter featuring the ratio of effective slopes and surface anisotropy (SAR) to more efficiently collapse ΔU^+ and $\Delta\Theta^+$ on their specific dataset. Insights into Pr regime influence on roughness-enhanced turbulent transport have been explored by Garg and Kadivar (2025), who studied surfaces with Gaussian profiles in the range $Re_b = 4000{-}15000$ and $Pr = 1{-}7$. Increasing Pr was found to improve thermal performance without affecting friction, yielding Reynolds analogy efficiencies greater than unity for $Pr \geq 3$ and motivating a Prandtl-dependent correlation. Recently, Secchi et al. (2025) introduced a framework for assessing the Reynolds analogy in turbulent forced convection over rough walls, linking the description of the time-averaged total mechanical energy and the transported scalar.

The unresolved disparity between momentum and heat transfer on rough walls highlighted from these studies is relevant for several engineering fields, including ice accretion, in which the predictive capability of roughness-induced heat transfer is needed for proper modeling of relevant phenomena. Within the context of aircraft icing, surface roughness is considered a critical parameter influencing convective heat transfer and consequently ice accretion rates, as summarized by Guardone et al. (2025). State-of-the-art icing codes employ modified Reynolds analogy formulations to estimate heat transfer at the ice–air interface (Beaugendre et al., 2003; Wright et al., 2022; Donizetti et al., 2025). However, their accuracy remains limited, especially for glaze ice cases, where convective heat transfer plays a significant role in determining local ice growth. Yang et al. (2023) adopted a zonal approach to investigate the local impact of ice roughness, though their analysis was restricted to skin-friction characterization. DNS of realistic ice scans were performed in Hu et al. (2024) and compared to Wall-Modeled LES and RANS, while Sotomayor-Zakharov et al. (2025) and Zabaleta et al. (2025) validated with different strategies the LES of a thermal turbulent boundary layer over realistic ice roughness. Their setup could reliably reproduce measured convective heat transfer over laser-scanned, unwrapped iced airfoils, establishing LES as a suitable tool for exploring enhancement mechanisms and guiding model development. Building on this framework, Gaudioso et al. (2025) applied the setup of Sotomayor-Zakharov et al. (2025) to show that k_s-based correlations derived from iced-surface properties, while effective in capturing skin-friction effects in the fully rough regime, struggle to accurately describe heat transfer through $\Delta\Theta^+$. Moreover, Sotomayor Zakharov et al. (2025) demonstrated RANS inaccuracies with respect to LES in the description of skin friction and heat transfer, relating these mostly to the predictive capabilities of local flow separation and reattachment.

These efforts have advanced the understanding of rough-wall heat transfer by isolating the effects of roughness morphology, Reynolds number, and Prandtl number. Collectively, these studies highlight the importance of high-fidelity simulations for a better understanding of heat transfer on rough surfaces. In particular, to determine and quantify the relation between momentum and heat transfer in the presence of roughness towards improving existing rough-wall heat transfer models, both for icing and for a broader range of applications. The classical turbulence properties scaling, originally formulated for momentum transfer, has been conventionally extended to thermal (or scalar) transfer under the assumption of analogous transport mechanisms (Kadivar et al., 2021). It is clear however that the validity of this assumption is hindered by roughness presence, as momentum and scalar exchanges respond differently to surface geometry and flow separation, calling into question the applicability of the traditional scaling.

In the present work, a modified scaling for turbulent convective heat transfer on rough surfaces is proposed, building on the Cavity-Vortex model hypotheses. The scaling is based on the rationale, emerged in many previous findings, that pressure does not contribute to the growth of heat transfer on rough walls. Thus, a viscous-only scaling is retrieved for which a measurable, non-dimensional parameter is defined and linked to the Reynolds analogy definition on rough surfaces through the roughness Stanton number St_k^{-1}. Furthermore, the same parameter is employed to derive a correction for thermal log-layer shift analysis and recover a distribution with respect to the equivalent sand-grain roughness parameter which resembles the one exhibited by the roughness function ΔU^+. Although previous studies explored viscous shear analogies with heat transfer, the approach has not — to the authors' knowledge — been formulated as a global correction to the Reynolds analogy and to the thermal roughness function on rough walls, $\Delta\Theta^+$. Therefore, the novelty does not lie in identifying the Reynolds analogy breakdown, which is well documented, but in the definition of a global viscous-based velocity scale that restores a fully rough–type similarity for heat transfer on the set of analyzed surface morphologies. The paper is structured as follows: Section 2 introduces the reference hypotheses for the work, including the previous literature treatment, and the present problem methodology with its key definitions; Section 3 describes the numerical databases used for the analysis, and the required data processing for the outputs; Section 4 presents the investigation outcomes and related discussion, while Section 5 draws conclusions and potential perspectives of the work.

2. Methodology

2.1. The CV heat transfer model

Based on the Cavity-Vortex (CV) hypothesis proposed by Owen and Thomson (1963) and elaborated by Dipprey and Sabersky (1963), heat transfer at the wall is driven by coherent flow structures such as hairpin and horseshoe vortices. This theory is based on the fully rough flow regime, in which drag becomes independent of viscous effects and the mean flow is assumed to be unaffected by viscosity. A further assumption is that the roughness elements are densely packed, leading to a sharp increase in shear stress and velocity as the flow approaches their crests, followed by a reduction while going down a trough. Consequently, the mean flow is prevented from penetrating into the cavities between roughness elements, and the roughness is modeled as a sublayer of strongly sheared flow. Within this sublayer, the streamwise velocity varies by an amount of order u_τ across a distance comparable to k_s (Kadivar and Garg, 2025). To model the wall heat flux q_w, Dipprey and Sabersky (1963) proposed:

$$q_w = \rho c_P u_\tau (T_w - T_k) St_k \tag{4}$$

where T_w is the wall temperature, T_k the temperature at the outer edge of the roughness sublayer, and St_k the roughness Stanton number, a term that acts as an inverse thermal resistance to the heat flow due to finite temperature drop in the roughness cavities as well as between and around roughness elements. Based on scaling arguments, Owen and Thomson (1963) derived a possible relation for St_k:

$$St_k = \frac{1}{\alpha_k}(k_s^+)^{-c} Pr^{-m} \tag{5}$$

where α_k is a constant value dependent merely on the roughness type, while exponents c and m depend on both molecular and turbulent diffusivities in the sublayer. Authors proposed different sets of coefficients for a St_k^{-1} relation based on the type of roughness investigated. For example, Owen and Thomson (1963) proposed $\alpha_k = 0.52$, $c = 0.45$, and $m = 0.80$ using u_τ as velocity scale. Differently, Dipprey and Sabersky (1963) employed the velocity scale at the roughness height $u_g = Bu_\tau$, with $B = 8.5$ for the fully rough regime, to obtain a different set of coefficients, i.e. $\alpha_k = 5.19$, $c = 0.20$, and $m = 0.44$. In so doing, they introduced the concept of cavity Stanton number St_c which is analogous to St_k, but based on u_g. Moreover, a roughness similarity function was defined which resembles St_k^{-1}, and it is indeed closely related to it through the turbulent Prandtl number and the fully rough regime constant B:

$$g_k = \alpha_c (k_s^+)^c Pr^m \quad \Rightarrow \quad St_k^{-1} = g_k - Pr_t B \tag{6}$$

Roughness induces substantial local pressure gradient variations, causing significant alterations to the Reynolds analogy. Indeed, it can be analytically shown (Dipprey and Sabersky, 1963) that St_k plays a role into the Reynolds analogy factor RA definition for rough surfaces:

$$RA = \frac{1}{Pr_t + \sqrt{\frac{c_f}{2}}\, St_k^{-1}} \tag{7}$$

From different definitions of St_k^{-1} arise disparate RA models tailored to specific roughness applications, as summarized in Kadivar and Garg (2025). In their work, the performance of such models is reviewed, while it emerges the application-specific nature of St_k^{-1} estimation according to the parameters entering Eq. (5).

2.2. Modified heat transfer scaling

Observing Eq. (4), it is evident that the heat flux would be increasing with St_k, or, equivalently, decreasing with St_k^{-1}. As k_s^+ increases for a given Pr, St_k^{-1} would eventually increase, entailing a higher thermal resistance to heat transfer across the roughness sublayer. Indeed, according to CV hypotheses, highly packed roughness elements would obstacle the mean flow to exchange momentum and heat with the flow trapped in between protrusions. This aspect is associated as well to the already mentioned growth in local pressure drag, which finds no analog contribution in convective heat transfer (Kadivar and Garg, 2025). On the other hand, the competing increase in u_τ for higher k_s^+ would drive an increase of q_w. While the CV model is linked to observed flow physics, its empirical basis is reflected in the estimation of St_k^{-1}, which would rely on an accurate k_s^+ model derived from surface geometrical features. However, as shown for example by the ice roughness study of Gaudioso et al. (2025), the choice of a representative k_s^+ is not trivial and could be case-specific.

On the basis of these observations, a modified thermal scaling is proposed and related to the CV model, in order to derive results which could be directly linked to classical Reynolds analogy and roughness shifts formulations. The underlying assumption is that eliminating the pressure contributions associated with local friction on rough surfaces compensates for the lag of thermal convection with respect to momentum transfer. However, differently from previous approaches (see for example Zhong et al. (2023), the viscous shear is not simply obtained by removing the pressure component from the classical wall-shear definition $\tau_w = \tau_x - p \cdot \eta_x$. Instead, the viscous shear stress magnitude is employed, which accounts for all viscous wall shear components. By incorporating this global viscous contribution along corrugated walls, a modified friction scale can be defined, which is expected to provide a closer analogy with heat transfer and to yield a more consistent scaling of turbulent profiles. To this end, a non-dimensional parameter G is introduced to quantify the relative significance of total shear (viscous and pressure) compared with purely viscous shear. Owing to its physical interpretation, this parameter can be directly linked to St_k^{-1}, thereby enabling verification of the proposed hypothesis and its integration within the CV model. Importantly, the proposed definition may require knowledge of the surface geometry, but an explicit link with equivalent sand roughness height k_s is left for future investigation.

Firstly, a modified friction velocity u_τ^* is introduced in Eq. (9) by considering the total viscous shear τ_v at the wall (Eq. (8)), computed from the components τ_x, τ_y, and τ_z of the viscous shear vector $\tau_i = \tau_{ij} n_j = 2\mu S_{ij} n_j$, where n_j is the outward unit normal to the wall and S_{ij} indicates the strain-rate tensor of a Newtonian fluid under the incompressibility assumption.

$$\tau_v = \sqrt{\tau_x^2 + \tau_y^2 + \tau_z^2} \tag{8}$$

$$u_\tau^* = \sqrt{\tau_v / \rho} \tag{9}$$

From this value, G is built as a ratio of friction velocity scales:

$$G = \frac{u_\tau}{u_\tau^*} \tag{10}$$

Finally, the definition of u_τ^* implies a modified friction temperature as well:

$$T_\tau^* = \frac{q_w}{\rho c_P u_\tau^*} \quad = G\, T_\tau \tag{11}$$

The superscript "*" will be used to denote turbulent properties scaling using these new friction values. It must be noted that the modified velocity scale does not discard pressure effects from the flow, while simply removing them from the wall-based normalization. Pressure-driven motions still affect the scalar field indirectly through their influence on the turbulence and the mean flow. The viscous wall shear stress exerted on the surface can therefore be regarded as a direct outcome of the local flow dynamics and pressure-induced separation, since recirculating regions are characterized by reduced wall-shear-stress magnitude, and the latter is associated with lower heat transfer.

The assumptions underlying the CV model indicate that the parameter G represents an appropriate non-dimensional quantity to characterize the physical processes within the roughness sublayer. An increase in G is expected to correspond to an increase in the thermal resistance of the flow. This trend is consistent with the interpretation that a larger pressure contribution to shear implies the generation of stronger wakes by the roughness elements, which in turn enhance recirculation. Such recirculating motions contribute to the thermal resistance to heat transfer, expressed by St_k^{-1}. On this basis, a relation between G and St_k^{-1} can be anticipated, thereby enabling verification of the proposed hypothesis and its integration within the CV model.

Another aspect arising from this treatment can be directly inferred from the proposed definition of G and is related to roughness-shift scaling (see Eqs. (2) and (3)). The conventional approach links ΔU^+ and $\Delta\Theta^+$ to the equivalent sand-grain roughness k_s^+. As previously noted, the behavior of $\Delta\Theta^+$ in the fully rough regime exhibits a flattening, reflecting the lagged increase in heat transfer due to the disproportion introduced by pressure relative to friction. For complex morphologies, k_s^+ models struggle even to collapse $\Delta\Theta^+$ onto consistent trends (Gaudioso et al., 2025). Here, G serves as a parameter quantifying this disproportion, thereby connecting to the observed discrepancy between ΔU^+ and $\Delta\Theta^+$. In this context, the disproportion manifests within the temperature profile and its associated scaling. Consequently, it is proposed that a rescaling of θ through T_τ^* would reveal a dependence of the thermal shift in which the pressure contribution is effectively restored, yielding a fully rough asymptotic behavior in k_s^+ analogous to that observed for ΔU^+.

To explore this scenario, from the definition of a modified friction temperature (Eq. (11)), it is possible to derive a re-scaled temperature profile θ^*:

$$\theta^* = \frac{Pr_t}{\kappa G}\log y^+ + \frac{C_\theta}{G} - \frac{\Delta\Theta^+}{G} \tag{12}$$

Formally, this rescaling would act as a modification of the slope and the intercept of the log-law. This re-scaled profile can be exploited to compute a modified roughness shift with respect to the asymptotic log-law for smooth walls, at a specific y_c^+. The wall-normal height y_c^+ should be corresponding to the evaluation coordinate for $\Delta\Theta^+$ from Eq. (3), thus falling in the log-layer of the profile. A modified temperature roughness shift $\Delta\Theta^*$ can be computed by subtracting $\theta^*(y_c^+)$ from the corresponding smooth log-layer value:

$$\Delta\Theta^* = \left[\frac{Pr_t}{\kappa}\log y_c^+ + C_\theta\right] - \theta^*(y_c^+) \tag{13}$$

Some manipulation to Eq. (13) leads to the following relation between $\Delta\Theta^*$ and $\Delta\Theta^+$,

$$\Delta\Theta^* = \Delta\Theta^+ + \left(1 - \frac{1}{G}\right)\theta^+(y_c^+) \tag{14}$$

in which G appears as a relative weighting factor for $\theta^+(y_c^+)$, namely the rough log-layer temperature value. It can be noted that $\Delta\Theta^* \to \Delta\Theta^+$ for $G \to 1$, recovering the classical definition of shift. For $G > 1$, the multiplying factor $(1 - 1/G)$ assumes values between 0 and 1, modulating the importance of pressure contribution to friction and transferring it to $\Delta\Theta^*$.

3. Numerical databases

For the present analysis, two main rough surfaces types are considered, which make part of different numerical datasets. The first one consists of the DNS of turbulent forced convection on sinusoidal walls, while the second is derived from the LES of turbulent thermal boundary layers on iced topologies obtained from experimental scans. The investigation of these substantially different set of rough surfaces delivers a higher grade of robustness to the tested approach, as cleared out later in the manuscript.

3.1. Homogeneous sinusoidal roughness

The sinusoidal walls refer to the DNS of MacDonald et al. (2019), who analyzed how roughness affects turbulent forced convection in minimal channels. The 3D sinusoidal profile follows the present equation:

$$k(x,z) = k_a \cos\frac{2\pi x}{\Lambda_x}\cos\frac{2\pi z}{\Lambda_z} \tag{15}$$

where k_a is the amplitude of the oscillations, while the wavelengths are spatially uniform and set as $\Lambda_x = \Lambda_z = 7.07\,k_a$. A sample sinusoidal patch used as minimal channel wall is reported in Fig. 1. In this case, the roughness is spatially uniform and controlled by its amplitude with respect to the boundary layer height, thus not requiring any statistical characterization.

The dataset is obtained at different friction Reynolds number Re_τ, covering the transitional and fully rough regime. A second-order energy-conserving finite volume code is used to solve the incompressible Navier–Stokes equations for the velocity vector $\boldsymbol{u}$, and the transported scalar $\theta = T_w - T$:

$$\nabla\cdot\boldsymbol{u} = 0, \tag{16a}$$

Table 1
Set of minimal rough-wall channel simulations from (MacDonald et al., 2019).

Re_τ	h/k_a	k_a^+	λ^+	L_x^+	L_z^+	ΔU^+	$\Delta\Theta^+$
395	36	11.0	78	1086	155	4.0	1.8
395	18	21.9	155	1086	155	6.5	3.0
590	18	32.8	232	1390	232	8.2	3.9
720	18	40.0	282	1414	282	9.0	4.2
1200	18	66.7	471	1414	471	10.3	4.5
1680	18	93.3	660	1979	660	10.9	4.3

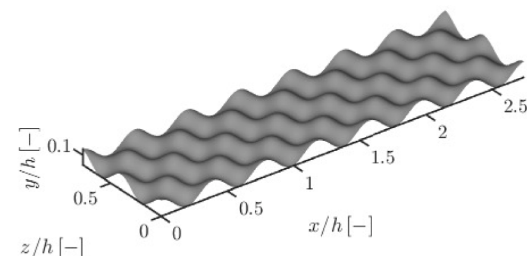

Fig. 1. Sinusoidal surface sample from MacDonald et al. (2019).

$$\frac{\partial\boldsymbol{u}}{\partial t} + \nabla\cdot(\boldsymbol{u}\boldsymbol{u}) = -\frac{1}{\rho}\nabla p + \nu\nabla^2\boldsymbol{u} + \boldsymbol{F_u}, \tag{16b}$$

$$\frac{\partial\theta}{\partial t} + \nabla\cdot(\boldsymbol{u}\theta) = \frac{\lambda}{\rho\,c_P}\nabla^2\theta + F_\theta. \tag{16c}$$

Here, $\boldsymbol{F_u}$ and F_θ are forcing terms corresponding to streamwise pressure and temperature gradients, adjusted to keep the bulk flow velocity and temperature constant at all times. The study fixes a molecular Prandtl number $Pr = 0.7$, and employs a no-slip, isothermal wall ($\theta_w = 0$). A body-fitted grid with fine resolution is used to discretize the sinusoidal surface, stretched in wall-normal direction.

Key geometry and simulation parameters are reported in Table 1, while more details can be found in MacDonald et al. (2019). The channel streamwise and spanwise extensions are reported as L_x^+ and L_z^+, evidencing the minimal channel application. Moreover, computed roughness log-layer shifts are included. The channel half-height h is set based on the fixed ratio $h/k_a = 18$ for all cases, with exception for the first one, which has $h/k_a = 36$. According to the authors, this was included to ensure a minimum $Re_\tau \geq 395$. Following the original analysis, this case was only considered for roughness shifts investigation, while being excluded from the bulk St estimation (later reported in Table 4).

3.2. Heterogeneous ice roughness

The set of complex ice topologies has been analyzed in the numerical setup developed and validated by Sotomayor-Zakharov et al. (2025), who performed zero-pressure-gradient (ZPG) simulations of experimental, unwrapped iced airfoil scans. The study verifies and validates the embedded LES approach as an accurate tool for the estimation of skin friction and heat transfer enhancement caused by realistic ice roughness, comparing simulation results with experimental measurements from McCarrell et al. (2018). The reference study solves the incompressible Navier–Stokes Eqs. (16a)–(16c) for the velocity vector $\boldsymbol{u}$ and the passive scalar $\theta = T_w - T$, with no external forcing ($\boldsymbol{F_u} = \boldsymbol{0}$, $F_\theta = 0$). Sotomayor-Zakharov et al. (2025) embedded the LES region around roughness, using the WALE subgrid model (Nicoud and Ducros, 1999) with $C_w = 0.325$, while modeling turbulence elsewhere by means of the SST k-ω model (Menter, 1994). No viscous heating is considered due to low flow speeds, and subgrid and turbulent Prandtl number values were fixed to $Pr_{sgs} = 0.85$ $Pr_t = 0.85$. The study considered an isothermal wall, keeping T_w constant while discarding conduction effects, and thoroughly addressing the implication of this modeling choice. Ice roughness is discretized by means of a body-fitted, Cartesian grid verified through a mesh independence study.

Table 2
Conditions and flow properties TBL simulations from Sotomayor-Zakharov et al. (2025).

U_∞ [m/s]	ρ [kg/m^3]	μ [Pa s]	L [mm]	Re_L [–]
6.672	1.124	$1.858 \cdot 10^{-5}$	952.5	$3.85 \cdot 10^5$
T_b [K]	ΔT [K]	c_P [J/kg K]	λ [W/m K]	Pr [–]
300	10	1007	$2.565 \cdot 10^{-2}$	0.729

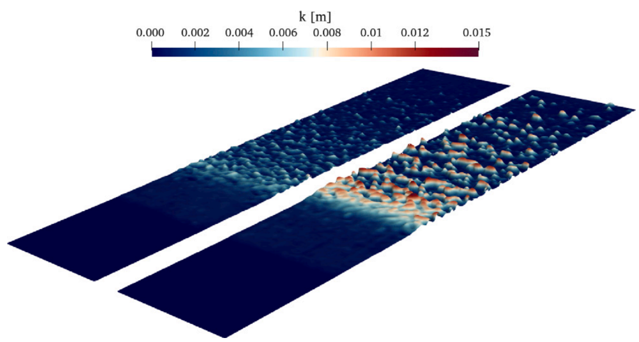

Fig. 2. Unwrapped iced airfoil scans tested in Sotomayor-Zakharov et al. (2025). Left: case 1; right: case 2.

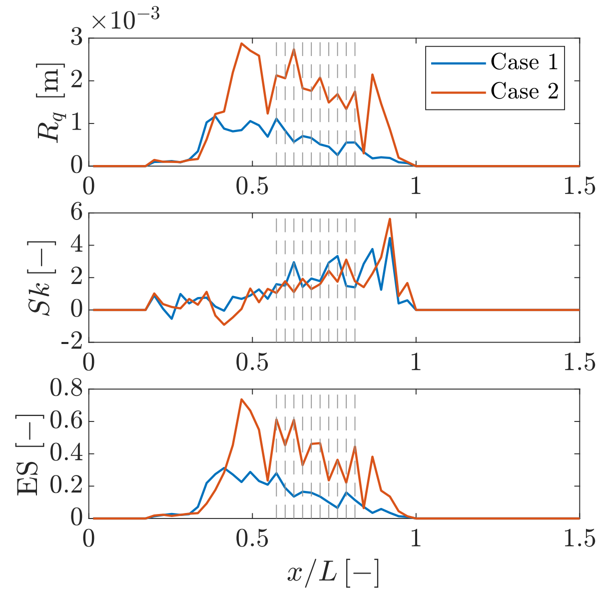

Fig. 3. Main geometrical parameters distributions along unwrapped ice scans.

The overall conditions for the turbulent boundary layer simulations performed by Sotomayor-Zakharov et al. (2025) are reported in Table 2, and match the experimental ones. For this dataset, the molecular Prandtl number is $Pr = 0.729$, aligned with the one employed by MacDonald et al. (2019). For reference, the surfaces are displayed in Fig. 2, where it can be noted that the suction side of the original airfoil scan was considered, with a smoothed frontal region allowing the proper development of the boundary layer onto the plate. Moreover, 2D distributions of root-mean-square roughness height R_q, skewness Sk, and effective slope ES are reported in Fig. 3, obtained by area-weighted evaluations of the roughness elevation profile at progressive streamwise locations. These parameters are defined in Eqs. (17a) - (17d), together with the mean roughness height k_m. Here, $k = k(x, z)$ represents the local surface elevation, and $S = \Delta x \cdot \Delta z$ is the local evaluation area.

$$k_m = \frac{1}{S}\int_S k\, dS \tag{17a}$$

$$R_q = \sqrt{\frac{1}{S}\int_S (k - k_m)^2\, dS} \tag{17b}$$

$$Sk = \frac{1}{S\,R_q^3}\int_S (k - k_m)^3\, dS \tag{17c}$$

$$\text{ES} = \frac{1}{S}\int_S \left|\frac{\partial k}{\partial x}\right| dS \tag{17d}$$

As evident from the distributions, the two analyzed geometries exhibit different R_q and ES, reflecting their respective accretion times, while Sk remains consistently positive, as is typical for roughness generated by surface deposits.

3.3. Data processing

The main numerical data processed in this work are derived from the DNS analysis of MacDonald et al. (2019) on sinusoidal roughness, and from the LES results of Sotomayor-Zakharov et al. (2025) on the irregular iced surfaces.

For the sinusoidal turbulent channel, the boundary layer height is constant and equal to the channel half-height h, and roughness is spatially homogeneous. Therefore, a global double average procedure can be employed by taking area-weighted integrals of time-averaged turbulent fields over the whole channel surface to extract relevant quantities for the analysis. In particular, viscous shear components in the three spatial directions and pressure shear are computed from available surface fields. Since minimal channels are considered, MacDonald et al. (2019) fitted the expected full-span velocity (U_f) and temperature (Θ_f) using the composite profile of Nagano and Tagawa (1988) to obtain the full-span bulk velocity $U_{bf} = \int_0^h U_f\, dy/h$ and mixed mean temperature $\theta_{bf} = \int_0^h U_f(\theta - \theta_w)\, dy / \int_0^h U_f\, dy$. From these definitions, the total c_f and St number can be derived:

$$c_f = \frac{2}{{U_{bf}^{+}}^2} \tag{18}$$

$$St = \frac{1}{U_{bf}^{+}\theta_{bf}^{+}} \tag{19}$$

Ultimately, roughness shifts are reported in MacDonald et al. (2019) (see Table 1), for which the evaluation is performed at the critical height $y_c^+ = 0.4\, L_z^+$. This distance is defined as the critical wall height above which the minimal channel profiles started to deviate from their physical log-law behavior. In the reference study, the virtual origin is taken as the mean sinusoidal roughness height, corresponding to $d = k_a$. The usage of minimal channels is systematically demonstrated to not affect the prediction of mean turbulent fields up to the log-layer, validating their use to study roughness functions. Additionally, the bulk properties estimation through full-span channel profiles fitting delivered convincing trends for smooth and rough cases, aligned with previous empirical models in the fully-rough regime.

Contrarily to forced convection over a uniformly rough wall, the analysis of surface fields for the turbulent boundary layer over irregular ice roughness is more complex, as the developing boundary layer presents an evolving thickness with respect to the local roughness height. As a direct consequence, flow quantities must be analyzed locally to assess the effect of roughness on turbulent properties. For the sake of the present analysis, only the data processing procedure will be outlined here, while the complete details can be found in the reference studies where the validation of the numerical setup (Sotomayor-Zakharov et al., 2025) and its extension to the analysis of equivalent sand grain roughness models (Gaudioso et al., 2025) are proposed. From the LES simulations, wall quantities τ_w and q_w are evaluated along the plate to derive c_f, St, and local wall-unit scales (u_τ, T_τ). As for surface statistics, the plate is divided into streamwise segments, each containing N mesh points over a projected area $S = \Delta x \times \Delta z$. Temporal means of pressure p_n, shear stress vector $\boldsymbol{\tau}_n$, and heat flux q_n at the wall are locally space-averaged to obtain τ_w and q_w as in Eqs. (20) and (21). The n-indexing highlights the single surface element quantity with outward normal vector $\boldsymbol{\eta}_n$. From double-averaged shear stress and heat flux, c_f and St are obtained through Eqs. (22) and (23). Note that the same nomenclature as the channel cases is used, as c_f and St are comparable quantities obtained from different setups.

$$\tau_w = \frac{1}{S}\sum_{n=1}^{N} S_n \left[\left(\boldsymbol{\tau}_n \cdot \boldsymbol{e}_x\right) - p_n \left(\boldsymbol{\eta}_n \cdot \boldsymbol{e}_x\right)\right] \tag{20}$$

$$q_w = \frac{1}{S}\sum_{n=1}^{N} S_n\, q_n \tag{21}$$

$$c_f = \frac{2\,\tau_w}{\rho\, U_\infty^2} \tag{22}$$

$$St = \frac{q_w}{\rho\, C_P\, U_\infty \Delta T} \tag{23}$$

Mean one-dimensional turbulent profiles, used to derive roughness shifts, are obtained via double-averaging over local planes, as done for example by Piomelli and Yuan (2013). In this way, each time-averaged field $\overline{\varphi}$ extracted from simulations is further averaged over x and z within a plate segment, using a fixed wall-normal distribution, as shown in Eq. (24).

$$\langle \varphi, (x_n, y)\rangle = \frac{1}{S}\int_{x_n-\frac{\Delta x}{2}}^{x_n+\frac{\Delta x}{2}} \int_{-\frac{\Delta z}{2}}^{\frac{\Delta z}{2}} \overline{\varphi}(x,y,z)\,dx\,dz \tag{24}$$

Spatial resolutions Δx and Δz are consistent with experimental (McCarrell et al., 2018) and numerical (Sotomayor-Zakharov et al., 2025) references; note that Δz spans the entire computational width. Following this method, profiles are extracted at selected x_n in the region $0.57 < x/L < 0.81$ (depicted in Fig. 3 with gray dashed lines) covering the fully developed turbulent boundary layer on top of roughness. Roughness shifts ΔU^+ and $\Delta\Theta^+$ are obtained from these profiles relative to smooth log-laws $u_s^+ = 1/\kappa \log y^+ + C$ and $\theta_s^+ = Pr_t/\kappa \log y^+ + C_\theta$, following the diagnostic method of Yuan and Piomelli (2015), where log-layers are identified from the plateau range of the diagnostic functions $K_u^+ = y^+(d\langle u\rangle^+/dy^+)$ and $K_\theta^+ = y^+(d\langle\theta\rangle^+/dy^+)$. The shifts are computed as:

$$\Delta U^+ = u_s^+(y_c^+) - \langle u\rangle^+(y_c^+) \tag{25a}$$

$$\Delta\Theta^+ = \theta_s^+(y_c^+) - \langle\theta\rangle^+(y_c^+) \tag{25b}$$

where y_c^+ is the evaluation height falling within the log-layer of the profile. For a developing boundary layer, y_c^+ might be slightly varying at different x_n. The distance y^+ is defined taking into account a wall origin displacement $d = k_m$ (see Eq. (17a)). It is worth underlining that the definition of d may influence the computation of the roughness shifts and the resulting value of y_c^+. However, the datasets analyzed here consistently apply a wall-origin displacement equal to the mean roughness height to both mean velocity and temperature profiles, thus ensuring a uniform impact on the introduced G-rescaling and preserving the consistency of the observed trends.

Based on the data-processing procedures adopted for the two numerical datasets under analysis, the parameter G is estimated as a globally averaged quantity for each sinusoidal-wall case, and as a locally averaged quantity for the irregular ice geometries, evaluated at the streamwise locations x_n. To compute G, the total viscous shear defined in Eq. (8) must first be evaluated from the available data. At least two approaches to estimate the space- and time-averaged value of the viscous shear, here conveniently indicated as $\langle\tau_v\rangle$, can be followed for the two setups:

- The first method consists in extracting the instantaneous magnitude of the viscous shear vector, and perform the double-averaging directly on such field. Therefore, at a given surface location $(x, y, z) = \boldsymbol{x}$ and time step t, the instantaneous field

$$\tau_v(\boldsymbol{x}, t) = \sqrt{\tau_x(\boldsymbol{x},t)^2 + \tau_y(\boldsymbol{x},t)^2 + \tau_z(\boldsymbol{x},t)^2} \tag{26}$$

  is computed. Double-averaging can be applied to this field as detailed above, firstly obtaining the time-averaged $\overline{\tau_v}(\boldsymbol{x})$, and then space-averaging over the target rough surface to get $\langle\tau_v\rangle$ (see Eq. (20) for TBL cases). The outcome delivers a viscous shear magnitude which includes local shear turbulent fluctuations coming from the three spatial components.
- The second approach discards the computation of an instantaneous viscous shear magnitude, while relying directly on time-averages of the spatial components $(\overline{\tau_x}(\boldsymbol{x}), \overline{\tau_y}(\boldsymbol{x}), \overline{\tau_z}(\boldsymbol{x}))$ to retrieve the time-averaged viscous shear magnitude field

$$\overline{\tau_v}(\boldsymbol{x}) = \sqrt{\overline{\tau_x}(\boldsymbol{x})^2 + \overline{\tau_y}(\boldsymbol{x})^2 + \overline{\tau_z}(\boldsymbol{x})^2}\,. \tag{27}$$

  Once again, the extracted $\overline{\tau_v}(\boldsymbol{x})$ can be space-averaged over the target rough surface with the procedure outlined above. In this way, the output is related to the coherent mean vector, but rules out fluctuating component effect because the single components undergo time-averaging before the effective estimation of $\langle\tau_v\rangle$.

While physically more consistent, the first approach requires the mean of the viscous shear vector magnitude derived by time-averaging Eq. (26), which in the present context is available only for the database on irregular roughness. The second approach will be adopted instead, and for the TBL cases on ice the error yielded by following this alternative method is demonstrated to be minimal in Appendix A. As pointed out above, for the channel cases the global area-weighted average over the whole sinusoidal wall delivers a single $\langle\tau_v\rangle$ estimate for each case listed in Table 1. For the turbulent boundary layer cases, similarly to Eq. (20), the spatial averages along the plate of viscous shear are taken as:

$$\langle\tau_v\rangle = \frac{1}{S}\sum_{n=1}^{N} S_n \sqrt{\overline{\tau_{x,n}}^2 + \overline{\tau_{y,n}}^2 + \overline{\tau_{z,n}}^2}, \tag{28}$$

and result in a streamwise distribution. The estimation of the total viscous shear delivers finally u_τ^*, G, and T_τ^* as formulated in Section 2, where $\tau_v = \langle\tau_v\rangle$. Note that Sotomayor-Zakharov et al. (2025) performed a grid sensitivity analysis demonstrating convergence of c_f and St, and this is expected to hold for surface flow properties derived in this study as u_τ^* and G.

4. Results

4.1. Relation between St_k^{-1} and G

In this section, the input data from all simulation sets are used to analyze the relation between the inverse of the roughness Stanton number St_k^{-1}, and the non-dimensional parameter G. The former can be estimated from the RA factor computed from simulations, simply by inverting Eq. (7). The computation of G, instead, is based on the formulation described in Section 2. Here, a relation in the form $St_k^{-1} = f(G)$ is sought, in order to link G to the Reynolds analogy formulation, and possibly identify its physical role with relation to the CV hypotheses. Importantly, for cases where k_s^+ can be hardly characterized, the ability of computing G from simulations would bypass such definition to deliver a RA estimate. The underlying form of the function $f(G)$ can be revealed by visually inspecting the graph in Fig. 4, where values across different roughness types and configurations are plotted, and a linear trend for $f(G)$ can be observed.

At this point, it is worth to point out that the limited dataset highlights the need for further analysis, encompassing a wider range of

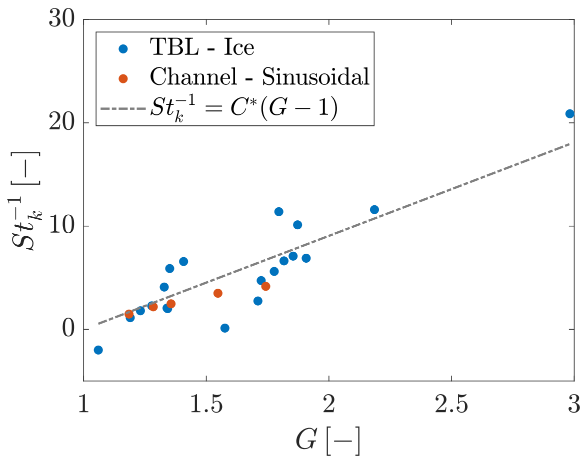

Fig. 4. Inverse roughness Stanton number plotted against G, with possible linear fit.

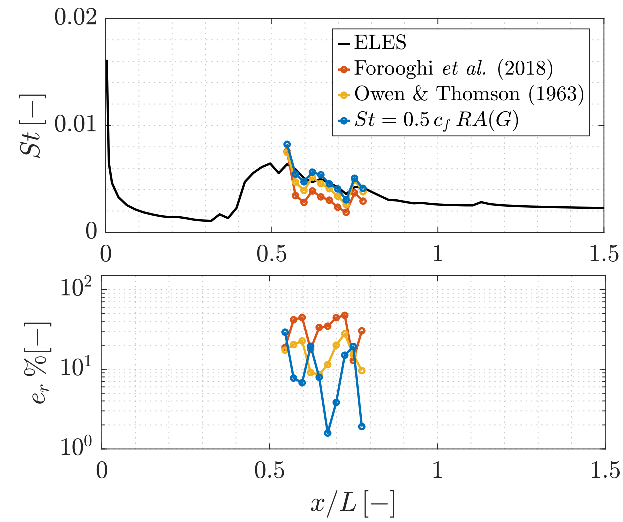

Fig. 5. Estimated St distributions at evaluation points for TBL case 1, based on different Reynolds analogy formulations (Forooghi et al. (2018a), Owen and Thomson (1963), and Eq. (30)). The computed St_{ref} trend is reported for comparison (Sotomayor-Zakharov et al., 2025). Relative errors at evaluation points x_n are shown in the lower panel.

roughness geometries and flow conditions. In such scenario, a unifying fit across different roughness types and Pr regimes cannot be pursued in the current study, leaving any further analysis on this aspect for future work. Nevertheless, the observed linear proportionality between St_k^{-1} and G indicates a potential dependence of the latter on near-wall flow dynamics, consistent with the CV theory framework. By assuming that the irregular ice and the sinusoidal wall could be described by the same $f(G)$, the following linear fit is delivered for the present data:

$$St_k^{-1} = f(G) = a^*(G-1) \tag{29}$$

with $a^* \simeq 9.05$. This value is totally indicative and must eventually be verified or adapted for other applications, while not affecting the baseline approach and its premises. Indeed, a^* can change based on specific morphology properties not investigated in this study, but also show a dependence on the Pr through St_k^{-1}. For example, additive manufactured roughness showed deviation of the heat transfer similarity function g_k approaching the fully-rough regime (Garg et al., 2024b,b).

As mentioned above, given the physical role of St_k^{-1}, the proportionality with G is expected. The current outcomes are indicating that, for a rough surface, G would quantify the averaged pressure gradient importance across roughness elements, which is directly linked to thermal transport lag effects.

4.2. Testing the modified RA formulation

Based on Eq. (7), a revised RA formulation including G can be now proposed:

$$RA(G) = \frac{1}{Pr_t + \sqrt{\frac{c_f}{2}}\,[a^*(G-1)]} \tag{30}$$

Since G is locally averaged for the TBL cases, a St estimation based on Eq. (30) can be derived and compared to the computed values. The resulting $St = 0.5\, c_f\, RA(G)$ would still rely on an accurate skin friction factor computation. For these simulations, a constant turbulent Prandtl number $Pr_t = 0.85$ is considered for the estimation of the turbulent thermal conductivity from the eddy viscosity (Sotomayor Zakharov et al., 2025). Eq. (30) delivers the St distributions shown in Figs. 5 and 6, where also the relative error $e_r = 100 \cdot (|St - St_{\mathrm{ref}}|)/St_{\mathrm{ref}}$ with respect to the values computed from LES is reported. A very close agreement is found in the turbulent region for most of the evaluation points x_n, and for both the tested geometries. To further assess this outcome, previous RA formulations are taken from literature to retrieve St based on friction values. The first is the RA correlation based on k_s^+ retrieved by Forooghi et al. (2018a), for which the Reynolds analogy factor of a rough surface can be estimated as

$$RA = RA_s\,[0.55 + 0.45\, e^{(-k_s^+/130)}], \tag{31}$$

where RA_s refers to the reference smooth Reynolds analogy value. Secondly, the Owen and Thomson (1963) relation for St_k^{-1} is considered, with $\alpha_k = 0.52$, $c = 0.45$, and $m = 0.80$ (see Eq. (5)). According to such formulations, to evaluate the resulting St distributions, a definition of k_s^+ is needed. The k_s^+ here introduced is based on the correlation proposed by Forooghi et al. (2017), displayed in Eq. (32), where k_z is the maximum peak-to-valley roughness height. This correlation was derived from a DNS database on irregular random roughness for ΔU^+ in the fully rough regime.

$$\frac{k_s}{k_z} = (0.67Sk^2 + 0.93Sk + 1.3)[1.07(1 - e^{-3.5\,\mathrm{ES}})] \tag{32}$$

The empirical St distributions are compared with the present G-based model in Figs. 5 and 6. For case 1, the correlation proposed by Owen and Thomson (1963) exhibits performance comparable to Eq. (30), accurately capturing the enhancement of St predicted by the simulations in the turbulent region. For the same geometry, the model by Forooghi et al. (2018a) reproduces the overall St trend, but systematically underestimates the numerical results. In case 2, characterized by larger roughness heights and higher k_s^+, the model based on Eq. (30) maintains a consistent prediction of the St distribution, whereas the other correlations show significantly larger deviations from the LES reference.

An overview of the model performance is resumed in Table 3, in which the mean relative error, $\langle e_r \rangle$, and its maximum value, $\max[e_r]$ across the x_n locations are indicated. Mean errors delivered from Forooghi et al. (2018a) model are similar across cases, while a greater sensitivity to local friction peaks is suggested by the maximum errors, which experience a significant growth. Nevertheless, as noted by previous assessments (Peeters and Sandham, 2019; Gaudioso et al., 2025), it is worth to underline that this correlation has been derived on a DNS dataset constituted mostly by regular roughness samples which may differ consistently from the present roughness type. As anticipated, the model from Owen and Thomson (1963) reveals an accurate prediction of St trends in the turbulent region for case 1, justifying its usage for heat transfer modeling on irregular roughness

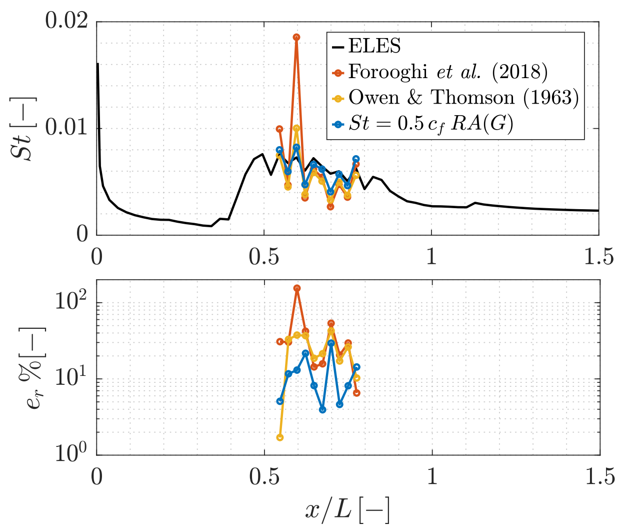

Fig. 6. Estimated St distributions at evaluation points for TBL case 2, based on different Reynolds analogy formulations (Forooghi et al. (2018a), Owen and Thomson (1963), and Eq. (30)). The computed St_{ref} trend is reported for comparison (Sotomayor-Zakharov et al., 2025). Relative errors at evaluation points x_n are shown in the lower panel.

Table 3
Comparison of mean and maximum model error in St distributions with respect to reference simulations.

RA model	TBL Case	$\langle e_r \rangle$ %	max $[e_r]$ %
Forooghi et al. (2018a)	1	32.6	47.4
Forooghi et al. (2018a)	2	39.8	154.7
Owen and Thomson (1963)	1	16.2	27.9
Owen and Thomson (1963)	2	24.6	42.7
Present (Eq. (30))	1	11.3	29.2
Present (Eq. (30))	2	12.0	29.4

in icing codes (Radenac et al., 2018). However, as roughness grows and elements obstruct the flow in case 2, the associated error increases. In contrast, for both geometries, the present formulation based on the parameter G is delivering accurate trends, as the mean and maximum error comparison indicates. Indeed, mean errors on St in the turbulent region are consistently lower than those associated to the empirical models used for comparison. This result constitutes only a verification for the present cases, while a finer tuning of $f(G)$ would need proper validation on wider databases. Nonetheless, this approach has demonstrated the potential of providing St estimations on irregular surfaces by knowledge of averaged friction and G values.

The Reynolds analogy factor RA can be retrieved for the sinusoidal channel following the formulation of Eq. (30), and using the c_f values reported in MacDonald et al. (2019). In this work, Pr_t shows minor differences with respect to smooth values at low friction Reynolds values, while for the two highest Re_τ an increase is observed near the roughness crest, followed by a sudden decrease. However, in accordance to Townsend's outer layer similarity hypotheses (Townsend, 1976), the smooth and rough Pr_t would collapse in the log-layer towards a constant value. Therefore, the RA factor is derived retaining a constant $Pr_t = 0.85$. Resulting St and relative errors with respect to values reported in the reference work (and computed using Eq. (19)) are summarized in Table 4. The errors of the estimation show acceptable limits, while evidencing a mismatch related to the fit $f(G)$, and underlying the possibility of model sensitivity to the type of roughness investigated.

Table 4
St estimate and relative errors for DNS of sinusoidal channel.

k^+	St_{ref} (MacDonald et al., 2019)	St	e_r%
21.9	0.0080	0.0089	12.15
32.8	0.0082	0.0090	9.54
40.0	0.0083	0.0088	5.85
66.7	0.0078	0.0078	0.80
93.3	0.0073	0.0067	7.94

It is remarkable that the verification holds for both the presented databases, which differs consistently in terms of topology and flow configuration. Still, this result lacks a systematic validation across roughness types and flow regime, which should be performed in order to assess its performance for a broader range of applications. The obtained estimates potentially do not require any specific k_s^+ model, aspect that represents the originality with respect to previous RA formulations on rough surfaces. On the other hand, while not investigated in this work, a possible G relation with k_s^+ needs to be explored.

4.3. Recovered fully-rough regime

The thermal shift correction derived in Section 2 has been applied to the present datasets, by previous evaluation of $\theta^+(y_c^+)$ values. The heights y_c^+ are evaluated at each x_n location for the plate based on the log-layer development (Gaudioso et al., 2025), while $y_c^+ = 0.4\,L_z^+$ for the sinusoidal channel (MacDonald et al., 2019). The resulting shifts distributions onto the iced surfaces are evaluated against the equivalent sand grain roughness of Forooghi et al. (2017), already presented in Eq. (32). In a simpler way, MacDonald et al. (2019) suggested $k_s = 4.1k_a$ for its sinusoidal wall based on ΔU^+ from DNS.

Results are displayed in Fig. 7 for the TBL ice roughness cases, and in Fig. 8 for the sinusoidal channel. The modified $\Delta\Theta^*$ is plotted against $k_s^* = k_s^+/G$, where the wall-units are scaled to account for G. Interestingly, the outcome highlights a very similar trend of $\Delta\Theta^*$, which departs from $\Delta\Theta^+$ to align instead with momentum trends quantified by velocity shifts. Forooghi et al. (2017) correlation is delivering an acceptable collapse of ΔU^+ towards the fully rough regime for both ice roughness geometries. No evident pattern is found by plotting $\Delta\Theta^+$, while a trend appears when including the proposed correction. The same reasoning holds for the data from MacDonald et al. (2019), in which $\Delta\Theta^*$ recovers a quasi-fully-rough behavior as seen for irregular roughness. This observation increases its robustness when considering the consistently different nature of the two setups analyzed, including the definition of k_s, while generalization requires additional validation on diverse morphologies and at different Pr.

Consistently with the hypotheses, the introduced non-dimensional parameter seems to restore, at least in an average sense, an analogy between heat transfer and momentum, which is testified by the close behavior of $\Delta\Theta^*$ and ΔU^+. As anticipated by previous observations, further assessment of the method on additional databases and refinement for enhanced practicability are needed, thereby establishing a basis for the development of improved models.

5. Conclusions

The present analysis introduces a modified scaling for describing the analogy between turbulent heat transfer and friction on rough walls. The formulation builds on the definition of modified friction quantities u_τ^* and T_τ^*, based on the total viscous shear, from which a non-dimensional parameter G naturally arises. This modified scaling through G, directly obtainable from simulations, is shown to restore the Reynolds analogy on rough walls in an averaged sense. The physical interpretation is connected to the absence of a heat-transfer counterpart to the local pressure gradient mechanism, which has long been

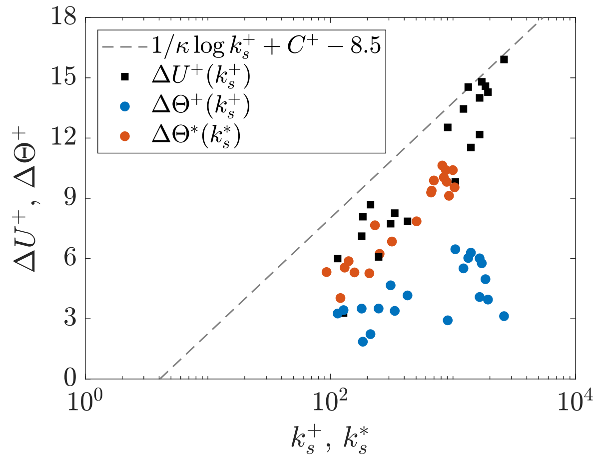

Fig. 7. Roughness shifts for TBL on irregular ice roughness. All data points are reported against k_s (Eq. (32)) scaled with respect to u_τ and u_τ^*.

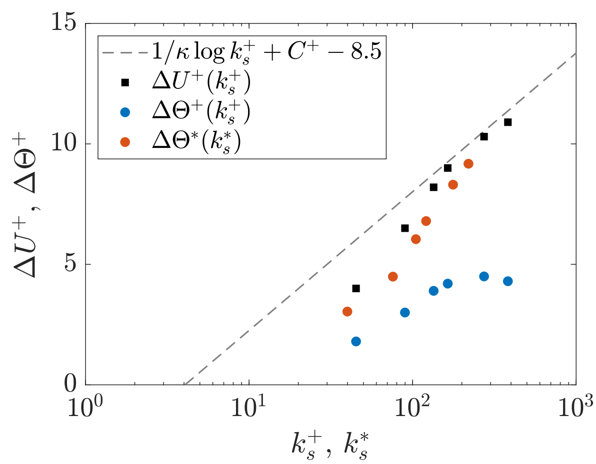

Fig. 8. Roughness shifts for sinusoidal channels reproduced from MacDonald et al. (2019). All data points are reported against $k_s = 4.1\,k_a$ (Eq. (32)) scaled with respect to u_τ and u_τ^*.

recognized as one of the main reasons why the analogy fails on rough substrates.

Two numerical databases are employed to support this hypothesis: an irregular ice roughness LES and a turbulent channel flow over sinusoidal roughness. Despite their differences in nature and roughness characteristics, both datasets are analyzed within a unified framework. First, G is related to rough Reynolds analogy factor RA formulations based on cavity vortex hypotheses, leveraging the roughness Stanton number St_k^{-1}. A proportionality between G and St_k^{-1} is consistently observed in both databases, and a fit is proposed to refine St number estimates. The predicted values display close agreement with numerical results, supporting the interpretation of G as a quantifier of thermal resistance, or thermal lag, relative to momentum transfer.

The analysis is then extended to the perspective of roughness-induced log-layer shifts. A correction to the classical $\Delta\Theta^+(k_s^+)$ scaling is proposed, based on averaged G values across both databases. The resulting $\Delta\Theta^*(k_s^*)$ exhibits a collapse much closer to that of momentum shifts $\Delta U^+(k_s^+)$, with reduced sensitivity to specific flow configurations.

In summary, the present results indicate that G can account for pressure-gradient effects in heat-transfer modeling through analogy with friction for the two rough surfaces considered. From a Reynolds-analogy perspective, the proposed formulation enables estimation of St from c_f and averaged flow properties computed over the true geometry. However, the limited number of roughness datasets and the restriction to a single Pr value prevent general conclusions. In this sense, the present study should be regarded as a first step towards a more general framework. Future work should investigate the dependence of G on surface topology, including its relation with k_s, and extend the analysis to additional roughness types, Prandtl numbers, and flow regimes to assess the robustness and generality of the approach.

CRediT authorship contribution statement

R. Gaudioso: Writing – original draft, Visualization, Project administration, Methodology, Investigation, Formal analysis, Data curation, Conceptualization. **D. Sotomayor-Zakharov:** Writing – review & editing, Supervision, Resources, Conceptualization. **M. Gallia:** Writing – review & editing, Supervision, Resources, Funding acquisition.

Declaration of competing interest

The authors declare that they have no known competing financial interests or personal relationships that could have appeared to influence the work reported in this paper.

Acknowledgments

R.G. has received funding from the European Union's Horizon Europe research and innovation program under the Marie Skłodowska-Curie grant agreement No 101072551 (TRACES). M.G. has received funding from the European Union's Horizon Europe research and innovation program under the Marie Skłodowska-Curie grant agreement No 101206621 (RESET).

Appendix. Assessment of surface-averaged viscous shear computation procedure

In the following, the two approaches for computing the averaged surface viscous shear presented in Section 3.3 are compared. The first method accounts for viscous shear fluctuations of each component at the wall, by extracting at each time step the instantaneous module of the viscous shear (see Eq. (26)). While this approach is physically more consistent, it requires knowledge of such instantaneous field $\tau_v(\boldsymbol{x}, t)$, an information only available for the database on irregular roughness. In contrast, the present treatment evaluates viscous shear from the time-averaged stress components, and subsequently computes their resultant after the simulation (see Eq. (27)). This alternative was the only viable option, due to data availability, for the sinusoidal channel of MacDonald et al. (2019). To quantify the difference between this simplified formulation (subscript 2) and the more consistent one (subscript 1), the relative error e_τ is introduced as

$$e_\tau = 100 \cdot \frac{|\langle\tau_{v,2}\rangle - \langle\tau_{v,1}\rangle|}{\langle\tau_{v,1}\rangle}, \tag{33}$$

where $\langle\tau_{v,1}\rangle$ and $\langle\tau_{v,1}\rangle$ are obtained using the two formulations presented in Section 3.3, with the first taken as the reference. The resulting error consists in a double-averaged distribution of the relative difference in viscous shear magnitude estimation onto the rough surfaces. The e_τ trends along the rough surface at x_n locations are shown in Fig. 9. As evident, the effect of the localized viscous shear differences becomes negligible, even if fluctuations effects may be locally considerable. Values remain below 2%, thereby justifying the use of approach 2 for both databases.

Data availability

Data will be made available on request.

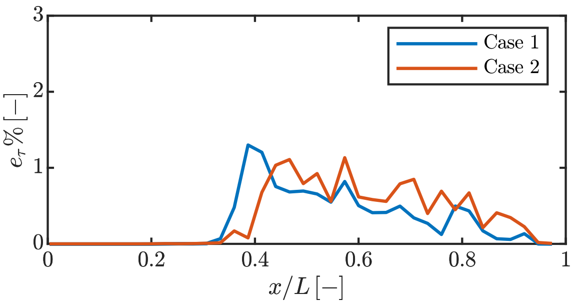

Fig. 9. Spatially averaged relative difference in viscous shear estimation over the rough plate.

References

Beaugendre, H., Morency, F., Habashi, W.G., 2003. FENSAP-ICE's three-dimensional in-flight ice accretion module: ICE3D. J. Aircr. 40 (2), 239–247. http://dx.doi.org/10.2514/2.3113.

Bons, J., 2005. A critical assessment of Reynolds analogy for turbine flows. J. Heat Transf. 127 (5), 472–485. http://dx.doi.org/10.1115/1.1861919.

Brutsaert, W., 1975. A theory for local evaporation (or heat transfer) from rough and smooth surfaces at ground level. Water Resour. Res. 11 (4), 543–550. http://dx.doi.org/10.1029/WR011i004p00543.

Dipprey, D.F., Sabersky, R.H., 1963. Heat and momentum transfer in smooth and rough tubes at various Prandtl numbers. Int. J. Heat Mass Transfer 6 (5), 329–353. http://dx.doi.org/10.1016/0017-9310(63)90097-8.

Donizetti, A., Bellosta, T., Rausa, A., Re, B., Guardone, A., 2025. Three-dimensional front-tracking technique for multistep simulations of aircraft icing. J. Aircr. 62 (2), 328–340. http://dx.doi.org/10.2514/1.C037933.

Flack, K.A., Schultz, M.P., 2010. Review of hydraulic roughness scales in the fully rough regime. J. Fluids Eng. 132 (4), 041203. http://dx.doi.org/10.1115/1.4001492.

Forooghi, P., Stripf, M., Frohnapfel, B., 2018a. A systematic study of turbulent heat transfer over rough walls. Int. J. Heat Mass Transfer 127, 1157–1168. http://dx.doi.org/10.1016/j.ijheatmasstransfer.2018.08.013.

Forooghi, P., Stroh, A., Magagnato, F., Jakirlić, S., Frohnapfel, B., 2017. Toward a universal roughness correlation. J. Fluids Eng. 139 (12), 121201. http://dx.doi.org/10.1115/1.4037280.

Forooghi, P., Weidenlener, A., Magagnato, F., Böhm, B., Kubach, H., Koch, T., Frohnapfel, B., 2018b. DNS of momentum and heat transfer over rough surfaces based on realistic combustion chamber deposit geometries. Int. J. Heat Fluid Flow 69, 83–94. http://dx.doi.org/10.1016/j.ijheatfluidflow.2017.12.002.

Garg, H., Kadivar, M., 2025. LES investigation of heat transfer in a tube with irregular roughness at moderate Prandtl numbers. Int. Commun. Heat Mass Transfer 169, 109931. http://dx.doi.org/10.1016/j.icheatmasstransfer.2025.109931.

Garg, H., Sahut, G., Tuneskog, E., Nogenmyr, K.-J., Fureby, C., 2024a. Large eddy simulations of flow over additively manufactured surfaces: Impact of roughness and skewness on turbulent heat transfer. Phys. Fluids 36 (8), http://dx.doi.org/10.1063/5.0221006.

Garg, H., Wang, L., Fureby, C., 2024b. Heat transfer enhancement with additively manufactured rough surfaces: Insights from large-eddy simulations. Phys. Fluids 36 (2), http://dx.doi.org/10.1063/5.0189115.

Gaudioso, R., Sotomayor-Zakharov, D., Gallia, M., 2025. Analysis of roughness correlations on ice geometries via embedded large-eddy simulation. AIAA J. http://dx.doi.org/10.2514/1.J066103, Article in advance.

Guardone, A., Bellosta, T., Donizetti, A., Gallia, M., 2025. Aircraft icing: Modeling and simulation. Annu. Rev. Fluid Mech. 58, http://dx.doi.org/10.1146/annurev-fluid-112723-062537.

Hantsis, Z., Piomelli, U., 2022. Effects of roughness on the turbulent Prandtl number, timescale ratio, and dissipation of a passive scalar. Phys. Rev. Fluids 7 (12), 124601. http://dx.doi.org/10.1103/PhysRevFluids.7.124601.

Hu, X., Agrawal, R., Zabaleta, F., Yang, X., 2024. Flow over ice roughness part I. Roughness heterogeneity. In: Proceedings of the Summer Program, Center for Turbulence Research. Stanford University, http://dx.doi.org/10.13140/RG.2.2.24804.08325, (in Preparation).

Kadivar, M., Garg, H., 2025. Turbulent heat transfer over roughness: a comprehensive review of theories and turbulent flow structure. Int. J. Thermofluids 26, 100967. http://dx.doi.org/10.1016/j.ijft.2024.100967.

Kadivar, M., Tormey, D., McGranaghan, G., 2021. A review on turbulent flow over rough surfaces: fundamentals and theories. Int. J. Thermofluids 10, 100077. http://dx.doi.org/10.1016/j.ijft.2021.100077.

Kasagi, N., Tomita, Y., Kuroda, A., 1992. Direct numerical simulation of passive scalar field in a turbulent channel flow. J. Heat Transf. 114 (3), 598–606. http://dx.doi.org/10.1115/1.2911323.

Kays, W.M., Crawford, M.E., 1993. Convective Heat and Mass Transfer, third ed. McGraw-Hill.

MacDonald, M., Hutchins, N., Chung, D., 2019. Roughness effects in turbulent forced convection. J. Fluid Mech. 861, 138–162. http://dx.doi.org/10.1017/jfm.2018.900.

McCarrell, J.L., Shannon, T.A., McClain, S.T., 2018. Convection from surfaces with ice roughness characterized at increasing accumulation times. In: 2018 Atmospheric and Space Environments Conference. p. 3016. http://dx.doi.org/10.2514/6.2018-3016.

Menter, F.R., 1994. Two-equation eddy-viscosity turbulence models for engineering applications. AIAA J. 32 (8), 1598–1605. http://dx.doi.org/10.2514/3.12149.

Nagano, Y., Tagawa, M., 1988. Statistical characteristics of wall turbulence with a passive scalar. J. Fluid Mech. 196, 157–185. http://dx.doi.org/10.1017/S0022112088002654.

Nicoud, F., Ducros, F., 1999. Subgrid-scale stress modelling based on the square of the velocity gradient tensor. Flow, Turbul. Combust. 62 (3), 183–200. http://dx.doi.org/10.1023/a:1009995426001.

Owen, P., Thomson, W., 1963. Heat transfer across rough surfaces. J. Fluid Mech. 15 (3), 321–334. http://dx.doi.org/10.1017/S0022112063000288.

Peeters, J., Sandham, N., 2019. Turbulent heat transfer in channels with irregular roughness. Int. J. Heat Mass Transfer 138, 454–467. http://dx.doi.org/10.1016/j.ijheatmasstransfer.2019.04.013.

Piomelli, U., Yuan, J., 2013. Numerical simulations of spatially developing, accelerating boundary layers. Phys. Fluids 25 (10), http://dx.doi.org/10.1063/1.4825033.

Pirozzoli, S., Bernardini, M., Orlandi, P., 2016. Passive scalars in turbulent channel flow at high Reynolds number. J. Fluid Mech. 788, 614–639. http://dx.doi.org/10.1017/jfm.2015.711.

Radenac, E., Kontogiannis, A., Bayeux, C., Villedieu, P., 2018. An extended rough-wall model for an integral boundary layer model intended for ice accretion calculations. In: 2018 Atmospheric and Space Environments Conference. p. 2858. http://dx.doi.org/10.2514/6.2018-2858.

Rowin, W.A., Zhong, K., Saurav, T., Jelly, T., Hutchins, N., Chung, D., 2024. Modelling the effect of roughness density on turbulent forced convection. J. Fluid Mech. 979, A22. http://dx.doi.org/10.1017/jfm.2023.1063.

Secchi, F., Gatti, D., Piomelli, U., Frohnapfel, B., 2025. A framework for assessing the Reynolds analogy in turbulent forced convection over rough walls. J. Fluid Mech. 1006, R3. http://dx.doi.org/10.1017/jfm.2025.1.

Sotomayor Zakharov, D., Gaudioso, R., Gallia, M., 2025. A comparison between LES and RANS simulations of realistic ice roughness. In: AIAA AVIATION FORUM and ASCEND 2025. p. 3209. http://dx.doi.org/10.2514/6.2025-3209.

Sotomayor-Zakharov, D., Gaudioso, R., Gallia, M., 2025. Embedded LES of a turbulent thermal boundary layer over ice roughness. Comput. & Fluids (ISSN: 0045-7930) 106652. http://dx.doi.org/10.1016/j.compfluid.2025.106652.

Thakkar, M., Busse, A., Sandham, N., 2017. Surface correlations of hydrodynamic drag for transitionally rough engineering surfaces. J. Turbul. 18 (2), 138–169. http://dx.doi.org/10.1080/14685248.2016.1258119.

Townsend, A., 1976. The Structure of Turbulent Shear Flow, second ed. Cambridge University Press.

Wright, W.B., Porter, C.E., Galloway, E.T., Rigby, D.L., 2022. GlennICE 2.1 capabilities and results. In: AIAA Aviation 2022 Forum. p. 3309. http://dx.doi.org/10.2514/6.2022-3309.

Yang, J., Stroh, A., Bagheri, S., Frohnapfel, B., Forooghi, P., 2025. Characterization of hydrodynamic and thermal properties of anisotropic irregular roughness. Int. J. Heat Fluid Flow 116, 109888. http://dx.doi.org/10.1016/j.ijheatfluidflow.2025.109888.

Yang, J., Stroh, A., Chung, D., Forooghi, P., 2022. Direct numerical simulation-based characterization of pseudo-random roughness in minimal channels. J. Fluid Mech. 941, A47. http://dx.doi.org/10.1017/jfm.2022.331.

Yang, J., Velandia, J., Bansmer, S., Stroh, A., Forooghi, P., 2023. A comparison of hydrodynamic and thermal properties of artificially generated against realistic rough surfaces. Int. J. Heat Fluid Flow 99, 109093. http://dx.doi.org/10.1016/j.ijheatfluidflow.2022.109093.

Yuan, J., Piomelli, U., 2015. Numerical simulation of a spatially developing accelerating boundary layer over roughness. J. Fluid Mech. 780, 192–214. http://dx.doi.org/10.1017/jfm.2015.437.

Zabaleta, F., Bornhoft, B., Jain, S., Bose, S., Moin, P., 2025. Large-eddy simulations of conjugate heat transfer in boundary layers over laser-scanned ice roughness. Phys. Rev. Fluids 10 (10), 104603. http://dx.doi.org/10.1103/fkg4-y3vf.

Zhong, K., Hutchins, N., Chung, D., 2023. Heat-transfer scaling at moderate Prandtl numbers in the fully rough regime. J. Fluid Mech. 959, A8. http://dx.doi.org/10.1017/jfm.2023.125.